Meteoritics & Planetary Science 33, 1101–1112 (1998)

Experimental studies of magnetite formation in the solar nebula

Y. HONG AND B. FEGLEY, JR.*

Planetary Chemistry Laboratory, Department of Earth and Planetary Sciences, Campus Box 1169, Washington University, One Brookings Drive, St. Louis, Missouri 63130-4899, USA
*Correspondence author's e-mail address: bfegley@levee.wustl.edu

(Received 1997 September 11; accepted in revised form 1998 March 24)
(Presented at the Workshop on Parent Body and Nebular Modification of Chondritic Materials at the University of Hawaii, Maui, Hawaii, USA 1997 July 16–19)

Abstract–Oxidation of Fe metal and Gibeon meteorite metal to magnetite *via* the net reaction 3 Fe (metal) + 4 H_2O (gas) = Fe_3O_4 (magnetite) + 4 H_2 (gas) was experimentally studied at ambient atmospheric pressure at 91–442 °C in H_2 and H_2-He gas mixtures with H_2/H_2O molar ratios of ~4–41. The magnetite produced was identified by x-ray diffraction. Electron microprobe analyses showed 3.3 wt% NiO and 0.24 wt% CoO (presumably as $NiFe_2O_4$ and $CoFe_2O_4$) in magnetite formed from Gibeon metal. The NiO and CoO concentrations are higher than expected from equilibrium between metal and oxide under the experimental conditions. Elevated NiO contents in magnetite were also observed by metallurgists during initial stages of oxidation of Fe-Ni alloys. The rate constants for magnetite formation were calculated from the weight gain data using a constant surface area model and the Jander, Ginstling–Brounshtein, and Valensi–Carter models for powder reactions. Magnetite formation followed parabolic (*i.e.*, diffusion-controlled) kinetics. The rate constants and apparent activation energies for Fe metal and Gibeon metal are:

$$\log_{10} k = -4.14(\pm 0.26) - \frac{4825(\pm 260)}{T} \text{ cm}^2 \text{ h}^{-1} \quad E_{act} = 92 \pm 5(2\sigma) \text{ kJ mol}^{-1}$$

$$\log_{10} k = -5.41(\pm 0.44) - \frac{4942(\pm 646)}{T} \text{ cm}^2 \text{ h}^{-1} \quad E_{act} = 95 \pm 12(2\sigma) \text{ kJ mol}^{-1}$$

These rate constants are significantly smaller than the parabolic rate constants for FeS growth on Fe metal in H_2S–H_2 gas mixtures containing 1000 or 10 000 ppmv H_2S (Lauretta *et al.*, 1996a). The experimental data for Fe and Gibeon metal are used to model the reaction time of Fe alloy grains in the solar nebula as a function of grain size and temperature. The reaction times for 0.1–1 μm radius metal grains are generally within estimated lifetimes of the solar nebula (0.1–10 Ma). However, the calculated reaction times are probably lower limits, and further study of magnetite formation at larger H_2/H_2O ratios, at lower temperatures and pressures, and as a function of metal alloy composition is needed for further modeling of nebular magnetite formation.

INTRODUCTION

Magnetite (Fe_3O_4) is found in varying abundance in carbonaceous chondrites (*e.g.*, Kerridge *et al.*, 1979; Hyman and Rowe, 1983; Krot *et al.*, 1995), interplanetary dust particles (IDPs) (Bradley *et al.*, 1984), and type-3 (unequilibrated) ordinary chondrites (*e.g.*, Nagahara, 1984; Krot *et al.*, 1997). The origin of magnetite in chondrites and IDPs is of considerable interest for several reasons. For example, if magnetite formed in the solar nebula, its presence in a meteorite or IDP then constrains the meteorite or IDP formation temperature to be at least as low as the magnetite formation temperature of ~400 K (Anders, 1971, 1972). Conversely, if magnetite formed on a parent body, its occurrence, morphology, age, *etc.*, constrain chemical and physical conditions and the timing of magnetite formation on the parent body (*e.g.*, Boström and Fredriksson, 1966; Kerridge *et al.*, 1979; Krot *et al.*, 1997).

However, the origin of magnetite in meteorites is quite controversial (Kerridge, 1970; Kerridge *et al.*, 1979; Krot *et al.*, 1995; Choi *et al.*, 1997). Condensation calculations predict that magnetite can form at ~400 K in the solar nebula by reaction of Fe alloy with water vapor (*e.g.*, Urey, 1952; Larimer, 1967; Grossman, 1972). Depending on the amount of Fe metal previously consumed by reaction with magnesium silicates to form FeO-bearing silicates, as much as 50% of all Fe (*i.e.*, Fe not in FeS) may be available for magnetite formation in the nebula. Because magnetite is formed by oxidation of preexisting metal grains, magnetite layers should grow on the metal grains and become thicker until all the remaining metal is consumed. Magnetite-rimmed metal grains have been observed in type-3 ordinary chondrites in some cases (*e.g.*, Nagahara, 1984) and could be nebular products. But in many other cases, the observed morphologies and mineral assemblages suggest that magnetite formed during low-temperature alteration on the meteorite parent body, in particular in CI carbonaceous chondrites (*e.g.*, DuFresne and Anders, 1962; Boström and Fredriksson, 1966; Jedwab, 1967, 1971; Kerridge *et al.*, 1979). The different magnetite morphologies and mineral assemblages found in different chondrites and even within one chondrite (*e.g.*, Orgueil, see Jedwab, 1971) probably indicate that not all of the magnetite assemblages in chondrites have the same origin.

During the past four decades, thermodynamic calculations and petrographic studies of meteorites have been used to discuss the origin of magnetite in meteorites. Another approach is to study the rate of Fe_3O_4 formation by reaction of Fe metal and alloy with H_2/H_2O gas mixtures:

$$3 \text{ Fe (metal)} + 4 \text{ H}_2\text{O (gas)} = \text{Fe}_3\text{O}_4 \text{ (magnetite)} + 4 \text{ H}_2 \text{ (gas)} \quad (1)$$

because this reaction is believed to produce magnetite in the solar nebula. If reaction (1), which occurs at low temperatures, cannot

proceed significantly over the nebular lifetime of 0.1–10 Ma (Podosek and Cassen, 1994), then it is unlikely that meteoritic magnetite formed in the solar nebula. Conversely, if reaction (1) proceeds appreciably over the nebular lifetime, then it is possible that at least some meteoritic magnetite formed in the solar nebula. In the latter case, the morphologies, minor and trace element contents of the magnetite formed *via* reaction (1) are of great interest for comparison with the different types of magnetite found in chondrites.

Fegley (1988) developed a simple collision theory (SCT) to estimate the reaction rates for the formation of some important volatile-bearing phases in chondrites (*e.g.*, hydrous silicates, magnetite, and troilite) under solar nebular conditions. For 0.1 μm radius spherical Fe metal grains, comparable in size to fine-grained meteorite matrix, the SCT models predict that the chemical lifetime for magnetite formation is ~320 000 years. The SCT models also predict that larger Fe metal grains are oxidized more slowly because of the smaller surface-to-volume ratios. Current estimates of the solar nebular lifetime are 0.1–10 Ma (Podosek and Cassen, 1994). Thus, as mentioned earlier, magnetite formation may or may not be kinetically inhibited over the lifetime of the solar nebula (Fegley, 1988, 1993; Fegley and Prinn, 1989).

As noted by Fegley (1988), the activation energy for wüstite formation at high temperatures (>860 K) in water-rich H_2O/H_2 mixtures (Turkdogan *et al.*, 1965)

$$0.947\ \text{Fe (metal)} + H_2O\ \text{(gas)} = Fe_{0.947}O\ \text{(wüstite)} + H_2\ \text{(gas)} \quad (2)$$

had to be used in the SCT modeling of magnetite formation because there were no kinetic data for reaction (1) at low temperatures. As a result, Fegley (1988) cautioned that firm conclusions regarding the kinetic favorability of magnetite formation in the solar nebula were premature and suggested that suitably designed experiments were necessary.

In this paper, we present the first results from an experimental study of magnetite formation kinetics at low temperatures in H_2 and H_2-He gas mixtures at ~1 bar total pressure. The mixtures have H_2/H_2O ratios of ~4–41. This work is analogous to our prior studies of FeS formation kinetics in H_2/H_2S gas mixtures (Lauretta *et al.*, 1996a,b, 1997) and is as important for constraining the rate of key gas–grain reactions in the solar nebula.

THERMODYNAMIC CALCULATIONS

We recalculated the magnetite formation temperature because of recent revisions in the solar elemental abundances (Grevesse and Noels, 1993) of H, O and C (2.82×10^{10} atoms, 2.09×10^7 atoms and 1.00×10^7 atoms, respectively, per 10^6 Si atoms) and in the thermodynamic data for magnetite and other iron oxides (Robie and Hemingway, 1995). The magnetite formation temperature was calculated using the net thermochemical reaction (1).

The equilibrium constant expression for reaction (1) is

$$K_1 = \frac{a_{Fe_3O_4} f_{H_2}^4}{a_{Fe}^3 f_{H_2O}^4} = \frac{a_{Fe_3O_4} P_{H_2}^4}{a_{Fe}^3 P_{H_2O}^4} \quad (3)$$

where a_i is the activity of phase i, f_i is the fugacity of gas i, and P_i is the partial pressure of gas i. Hydrogen and H_2O behave as ideal gases under nebular conditions, so their fugacities can be replaced by their partial pressures. Since reaction (1) consumes four moles of H_2O and produces four moles of H_2, the total pressure (P_T) cancels out of equation (3), and the equilibrium constant expression can be rewritten as

$$K_1 = \frac{a_{Fe_3O_4} X_{H_2}^4}{a_{Fe}^3 X_{H_2O}^4} \quad (4)$$

where X_i, the mole fraction of gas i, is equal to (P_i/P_T). Magnetite forms when its thermodynamic activity becomes unity. The magnetite activity is calculated by rearranging equation (4) to yield

$$a_{Fe_3O_4} = K_1 a_{Fe}^3 \left(\frac{X_{H_2O}}{X_{H_2}} \right)^4 \quad (5)$$

The equilibrium constant K_1 is calculated from the thermodynamic data tabulated by Robie and Hemingway (1995), and the activity of Fe is taken as unity (assuming pure Fe metal) or as 0.947 (assuming ideal solid solution and a solar composition Fe-Ni alloy).

The H_2O/H_2 ratio is calculated from solar elemental abundances, and two end-member cases were considered. At the low temperatures where magnetite forms, ~15% of all O is in rock (*i.e.*, SiO_2 + MgO). However, depending upon the distribution of C between CH_4 and CO, more or less of the remaining O is available to form water vapor. As discussed by Lewis and Prinn (1980) and Fegley and Prinn (1989), the reduction of CO to CH_4 in the solar nebula is probably kinetically inhibited over the lifetime of the solar nebula. Here we consider the two end-member cases: all C as CO (*i.e.*, complete kinetic inhibition) or all C as CH_4 (*i.e.*, no kinetic inhibition). If all C is present as CO, then the H_2O/H_2 ratio is $\sim 5.53 \times 10^{-4}$ (*i.e.*, $H_2/H_2O \sim 1808$). If all C is present as CH_4, then the H_2O/H_2 ratio is $\sim 1.26 \times 10^{-3}$ (*i.e.*, $H_2/H_2O \sim 794$).

Our calculated magnetite formation temperatures are listed in Table 1. Magnetite forms at 357 K, if all C is in CO, or at 384 K, if all C is in CH_4. The effect of ~6% Ni is minor and changes these temperatures by 1° or less. Our magnetite formation temperatures are 10–20° lower than the 370–400 K temperatures calculated previously (*e.g.*, Larimer, 1967; Grossman, 1972; Fegley, 1988) because of the changes in the H, O, and C solar elemental abundances and in the Fe_3O_4 thermodynamic data.

The range of magnetite formation temperatures (357–384 K) is also plotted on the Fe-O phase diagram in Fig. 1. The iron–wüstite, wüstite–magnetite, iron–magnetite, and magnetite–hematite phase boundaries in Fig. 1 are given by the reactions:

$$0.947\ \text{Fe (metal)} + H_2O\ \text{(gas)} = Fe_{0.947}O\ \text{(wüstite)} + H_2\ \text{(gas)} \quad (2)$$

$$3.17\ Fe_{0.947}O\ \text{(wüstite)} + 0.83\ H_2O\ \text{(gas)} = Fe_3O_4\ \text{(magnetite)} + 0.83\ H_2\ \text{(gas)} \quad (6)$$

$$3\ \text{Fe (metal)} + 4\ H_2O\ \text{(gas)} = Fe_3O_4\ \text{(magnetite)} + 4\ H_2\ \text{(gas)} \quad (1)$$

$$2\ Fe_3O_4\ \text{(magnetite)} + H_2O\ \text{(gas)} = 3\ Fe_2O_3\ \text{(hematite)} + H_2\ \text{(gas)} \quad (7)$$

which depend only on the H_2/H_2O ratio but not on the total pressure. Thermodynamic data for wüstite ($Fe_{0.947}O$), magnetite, and hematite were taken from Robie and Hemingway (1995). Figure 1 illustrates that magnetite and not another iron oxide is expected to form within the range of H_2O/H_2 ratios expected in the solar nebula. For comparison, we also plotted the conditions of our experimental runs on Fig. 1.

TABLE 1. Magnetite formation temperatures in the solar nebula.

H_2/H_2O ratio*	Pure Fe	Fe-Ni alloy
794 (CH_4)	384 K	383 K
1808 (CO)	357 K	357 K

*Based on elemental atomic abundances of H = 2.82×10^{10}, O = 2.09×10^7, and C = 1.00×10^7 per 10^6 Si atoms and consumption of 15% of O by rock (SiO_2 + MgO).

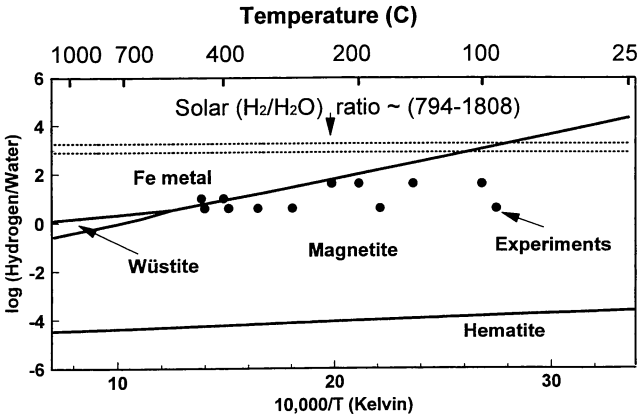

FIG. 1. The Fe-O phase diagram calculated using data in Robie and Hemingway (1995). The range of H_2/H_2O ratios in the solar nebula, which depends on the distribution of C between CO and CH_4 (Fegley and Prinn, 1989), is also shown. The intersection of the nebular H_2/H_2O ratios with the Fe_3O_4 phase boundary gives the range of magnetite formation temperatures in the solar nebula. The black dots show the positions of the experimental runs. Magnetite formation was observed in the runs represented by the dots under the Fe-Fe_3O_4 line, and no magnetite formation was observed in the two runs above the Fe-Fe_3O_4 line.

EXPERIMENTAL PROCEDURES

Starting Materials

The starting materials used in this work were high-purity (99.998%) Fe foil, high-purity (99.999%) Fe powder, small pieces of metal from the Gibeon IVA iron meteorite, and filings from Gibeon meteorite metal. The high-purity Fe foil and Fe powder were commercial products (Alfa AESAR, Ward Hill, MA), and the Gibeon meteorite was from the Planetary Chemistry Laboratory collection. Larger pieces of Gibeon meteorite metal were cut into smaller slices (0.5 × 0.5 × 0.075 cm) with a low-speed diamond saw, and Gibeon metal filings were collected during cutting. The small Gibeon slices were polished and cleaned before use. The commercial Fe metal foil was cut into 0.5 × 0.5 × 0.025 cm pieces and was also cleaned before use. The foils and meteorite pieces were handled with tweezers to avoid fingerprints. The geometric surface areas of the foils and pieces were measured with a micrometer. The Fe powder is a porous commercial product with a distribution of particle sizes (0.2–20 μm with an estimated nominal size of 5 μm). The Gibeon filings are irregularly shaped small metal particles (0.1–10 μm with an estimated nominal size of 2 μm). Particle sizes were calculated from scanning electron microscope (SEM) and optical microscope images of the powders.

Gas Mixtures and Analysis

Ultra high purity (UHP) grade H_2 (H_2, 99.999%) and He (He, 99.999%) were used to make H_2-He gas mixtures, and water vapor (H_2O) was introduced by bubbling H_2 or the H_2-He mixture through distilled water held at constant temperature in a water vapor saturator. Figure 2 is a schematic diagram showing the water vapor saturator and the rest of the experimental apparatus. This apparatus is analogous to that used in our experimental studies of iron sulfide formation (Lauretta *et al.*, 1996a,b, 1997).

Both H_2 and H_2O concentrations were regulated to obtain the desired H_2/H_2O ratios in the gas mixtures. The H_2 concentration was regulated from 10% to 100% by diluting H_2 with He using calibrated electronic mass flow controllers (Tylan Co.). The water vapor pressure in the H_2-He gas mixture was controlled by the temperature of the water vapor saturator, which was regulated to better than ±0.1 °C by a constant temperature circulating bath (VWR Scientific).

The H_2O concentrations in the gas mixture were analyzed by gas chromatography using a Hewlett Packard 5890 Series II Gas Chromatograph equipped with a Porapak Q column at 60 °C and a thermal conductivity detector. Ultra high purity grade He was used as the carrier gas at a flow rate of 100 cm^3 min^{-1}, and it was further purified with a He purifier (Alltech Co.). Gas lines connected the furnace exhausts to an automated gas sampling valve on the gas chromatograph allowing automated gas sampling and analysis. The H_2O peak area on the gas chromatograms was calibrated using the measured water uptake by Mg perchlorate [$Mg(ClO_4)_2$], which is an extremely efficient desiccant (Melville and Gowenlock, 1964). A gas mixture saturated with water vapor at 23.0 °C was passed through a $Mg(ClO_4)_2$ filled tube for 2 h at a flow rate of 100 cm^3 min^{-1} (STP). The observed weight gain of 0.265 g corresponds to a water vapor pressure of 0.0278 bar in the gas mixture, which is only 1% less than the saturated water vapor pressure of 0.0281 bar at 23.0 °C (Lide, 1996). The H_2O peak area on chromatograms of this saturated gas could be directly related then to the H_2O partial pressure in the gas mixture.

Figure 3 shows gas chromatograms of H_2 with and without H_2O vapor. The water vapor pressure measured by gas chromatography and the theoretical saturated water vapor pressure (Lide, 1996) at three different temperatures are listed in Table 2. The excellent agreement confirms that the gas mixtures passed through the water vapor saturator are saturated with water vapor at the preset temperatures. Gas mixtures with H_2/H_2O molar ratios of 41 and 4.1 were used in our experiments. These molar ratios remain the same in the furnace because the extent of H_2O dissociation is insignificant under the experimental conditions.

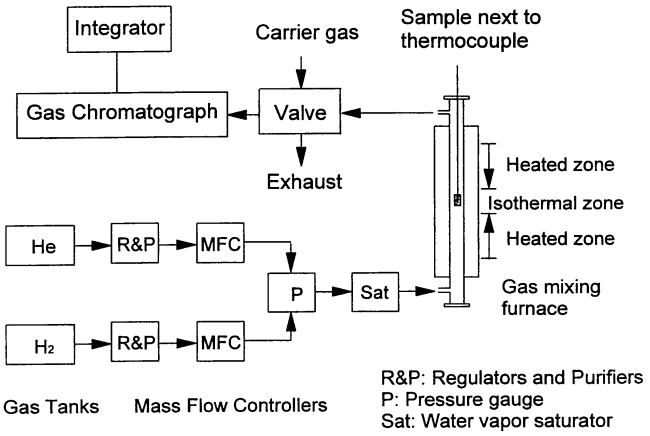

FIG. 2. Schematic diagram of the experimental apparatus used in this work.

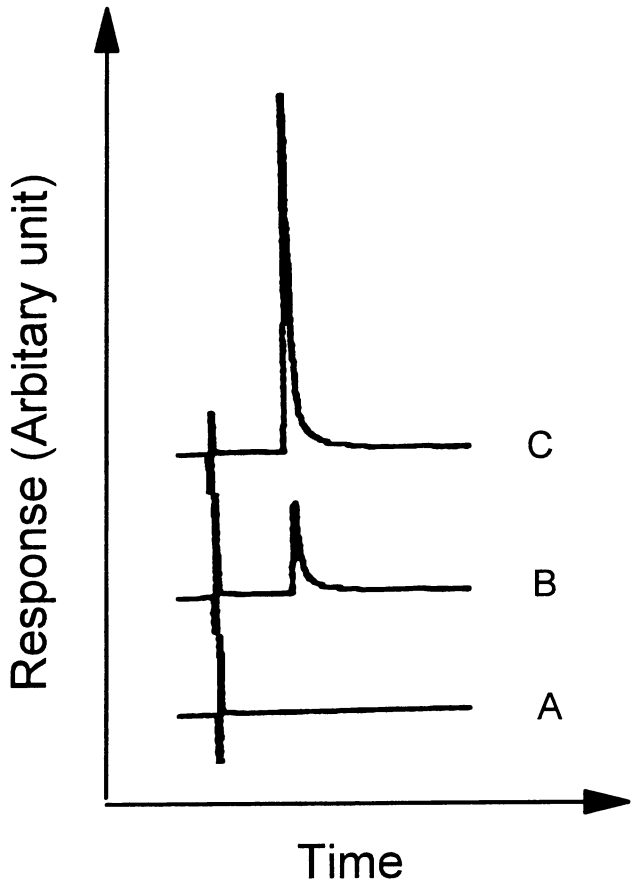

FIG. 3. Gas chromatograms of H_2 gas with and without water vapor. (a) H_2 without water vapor, (b) H_2 saturated with water vapor at 0 °C, and (c) H_2 saturated with water vapor at 10.0 °C.

Gas Mixing Furnace and Magnetite Formation

Magnetite formation was studied by heating Fe metal or Gibeon meteorite metal in H_2/H_2O gas mixtures at different temperatures for known periods of time. The Fe foils, Gibeon meteorite pieces, Fe powder, or Gibeon filings (1–2 mm thick layers of powder or filings) were placed in a ceramic boat, next to a calibrated Pt-$Pt_{90}Rh_{10}$ thermocouple in the isothermal zone of a Deltech horizontal tube furnace, and were annealed overnight in UHP grade H_2 at 450 °C. The thermocouple was calibrated against our laboratory reference thermocouple, which is calibrated at the melting point of Au. The reactions were started by passing 40 cm^3 min^{-1} (STP) H_2/H_2O flow over the sample. At the end of the reaction, the water-saturated gas flow was stopped, the sample was cooled in UHP grade He, and removed from the furnace. This is similar to the procedure used in our iron sulfide experiments (Lauretta *et al.*, 1996a,b). The starting materials and reacted samples were characterized by x-ray diffraction, electron microprobe analysis, scanning electron microscopy, gas adsorption surface area measurements, and weight gain measurements.

Sample Characterization

X-ray diffraction patterns of the starting materials and the reacted samples were obtained using a Rigaku vertical powder diffractometer with Cu Kα radiation (λ = 1.540598 Å) and Materials Data Incorporated (MDI) software. Calibration was done using Si powder (NIST 640b). The XRD patterns of the Fe foil and Fe powder are identical to that of a synthetic iron standard (JCPDS pattern 06-0696), and the XRD pattern of the Gibeon metal is analogous to that of kamacite (JCPDS pattern 37-0474) with a minor amount of taenite (JCPDS pattern 23-0297). The XRD patterns of the reacted products are discussed later.

TABLE 2. Measurements of water vapor pressure in gas mixtures, and comparison with the saturated vapor pressure.

Water saturator temperature (°C)	Water vapor pressure* (10^{-2} bar)	Saturated vapor pressure† (10^{-2} bar)
0.0	0.59	0.61
19.0	2.35	2.34
23.0	2.78	2.81

*Measured by gas chromatography and calibrated by measuring water uptake by Mg $(ClO_4)_2$.
†Data from Lide (1996).

Electron microprobe analyses of polished cross-sections of the reacted samples were done with the Washington University JEOL-733 electron microprobe equipped with advanced microbeam automation. The operating conditions are the same as described by Lauretta *et al.* (1996a), and Fe, Ni, and Co metal standards were used as the standards for Fe, Ni, and Co in the metal and oxides.

The unreacted Gibeon metal consists of larger areas of homogenous kamacite with ~7 wt% Ni, with narrow (5–10 μm) bands of kamacite–taenite (~15 wt% Ni) and scattered kamacite–taenite spots (<3 μm diameter with 15–35 wt% Ni). The average Fe, Ni, Co contents in the original sample were analyzed with a broad beam (~20 μm) and a 10 × 6 grid (with points 200 μm apart) giving an average atomic composition of $Fe_{91.5}Ni_{8.1}Co_{0.4}$ (91.1 wt% Fe, 8.4 wt% Ni, 0.4 wt% Co). For comparison, the corresponding atomic and weight ratios for another sample of Gibeon meteorite metal are $Fe_{91.9}Ni_{7.6}Co_{0.5}$ (91.5 wt% Fe, 7.9 wt% Ni, 0.5 wt% Co; Lauretta, 1997). The Fe, Ni, and Co concentrations of the residual metal and oxide in the reacted Gibeon filings were analyzed at one or more spots with a focused beam (~1 μm), but the oxide layers and the remnant metal grains were too small to do traverses.

Scanning electron microscope images of cross-sections of the starting materials and reacted samples and of some reacted Fe powders and Gibeon filings were also obtained.

Specific surface area measurements of the starting material and the reacted samples were done on a Quantasorb adsorption system (Quantachrome Co.). Samples weighing 50–200 mg were degassed at 280 °C overnight in inert gas. The amounts of N adsorbed by the solid at liquid nitrogen temperature were then measured under various relative N pressures (P/P_o), where P and P_o are the partial pressure of N in equilibrium with the solid sample, and the saturated N pressure at liquid nitrogen temperature, respectively. The BET equation was used to calculate the surface areas of the starting materials and reacted samples (Gregg and Sing, 1982). The Quantasorb adsorption system was calibrated with Al_2O_3 powder of known surface area. The specific surface areas measured in duplicate runs were within ±1% of the specified value (2.07 m^2 g^{-1}). The uncertainties in our surface area measurements are <±2%.

RESULTS AND DISCUSSION

Preliminary Experiments with Iron Foils and Meteorite Pieces

Our initial experimental runs were made using Fe foils and pieces of the Gibeon iron meteorite. This was done because our prior work

on iron sulfide formation showed that a great deal of information is obtained by studying the corrosion layers formed on metal pieces (Lauretta *et al.*, 1996a,b, 1997). However, we found that magnetite formation by reaction of Fe metal with H_2/H_2O gas mixtures is an extremely slow process, and it is almost impossible to get kinetic data in a reasonable amount of time by using Fe foils at high H_2/H_2O ratios (*i.e.*, low water vapor partial pressures) such as in the solar nebula. Thus, we concentrated on obtaining kinetic data from Fe powder and Gibeon meteorite filings, because the reaction rate is proportional to the surface area of the solid (Brown *et al.*, 1980). Because of their small size, the powder and filings have much larger specific surface areas (total surface area per gram sample, $m^2\ g^{-1}$) than the metal foils and are more rapidly converted to magnetite. For comparison, our surface area measurements show that the amount of Fe powder (150 mg) used in our experiments has a surface area ~500× larger than Fe foil (~0.1 m^2 *vs.* ~0.0002 m^2). However, days to weeks were still needed for significant conversion of the metal powder and filings to magnetite.

Despite the difficulties in obtaining kinetic data, our preliminary experiments showed that magnetite formation is reversible depending on the H_2/H_2O ratio. Pure Fe foil heated at 205 °C for 7 days in a gas mixture with an H_2/H_2O ratio of ~41 gained 60 $\mu g\ cm^{-2}$ and was partially converted to magnetite, verified by XRD. The calculated thickness of the magnetite layer was consistent with the thickness indicated by the oxide color (interference colors) on the surface of the reacted sample (Kubaschewski and Hopkins, 1953). This reacted sample returned to its original weight after being heated at 205 °C for 4 days in purified H_2 without H_2O. After this treatment, the sample showed the original metal appearance, the oxide color disappeared, and only Fe metal lines were observed in the XRD pattern. These observations show that magnetite was produced *via* Fe oxidation by water vapor and that the magnetite could be reduced to Fe metal when H_2O was not present in the H_2 gas mixture.

Experiments with Powder and Filings

Our subsequent experiments with Fe metal powder and Gibeon meteorite metal filings gave kinetic data for magnetite formation, which is summarized in Tables 3 and 4. However before considering the reaction rate, we first describe the chemistry, morphology, and microstructures of the reacted samples.

A typical x-ray diffraction pattern of the reacted Fe powder is shown in Fig. 4. The reflection lines of reacted samples include those of magnetite (JCPDS pattern 19-0629), in addition to those of the starting Fe powder. There is no sign of any other iron oxides (*e.g.*, hematite (JCPDS pattern 33-0664) or wüstite (JCPDS pattern 06-0615)) in the XRD patterns of the reacted products. Their absence is consistent with our experimental conditions and the Fe-O phase diagram (Fig. 1). The oxide does not show any preferred orientation, probably because Fe powder was used instead of Fe foil. For comparison, preferred orientations were observed in thicker (*e.g.*, >10 μm) sulfides formed by reaction of H_2S/H_2 mixtures with Fe foil (Lauretta *et al.*, 1996a).

Optical and scanning electron microscopy shows that the magnetite forms a layer on the outside of the metal powder and filings and also grows in any pores originally connected to the grain's original surface (Fig. 5a,b). The pores that do not contain any magnetite are internal pores that were not exposed to the gas mixture.

The commercial Fe powder is very porous, presumably as a result of the synthetic method. This porosity decreases with increasing conversion of Fe metal to magnetite. For example, Fig. 6a shows a SEM image of powder that is nearly unreacted (4.8% conversion to

TABLE 3. Experimental data for the oxidation of iron powder*.

Run number	Temp. (°C)	Time (h)	w_i (mg)	$100 \times \Delta w/w_i$ (%)	Fe reacted† (%)
H221	91	140.0	213.43	0.16	0.41
H230	91	306.5	152.88	0.26	0.68
H235	179	44.5	189.01	0.34	0.88
H220	179	140.0	96.92	0.67	1.75
H263	179	312.0	325.66	0.70	1.83
H234	281	44.5	175.56	3.27	8.57
H219	281	140.0	122.76	4.96	12.97
H232	281	306.5	141.59	7.08	18.54
H218	335	44.5	368.21	8.19	21.43
H226	390	1.0	153.81	1.84	4.81
H227	390	3.67	144.44	3.83	10.03
H228	390	7.0	119.09	6.38	16.71
H222	390	22.8	155.06	13.86	36.28
H223	390	42.7	158.42	18.44	48.27
H225	390	90.0	178.51	22.44	58.74
H224	390	140.0	168.97	26.32	68.91

*H_2/H_2O is 4.1, total pressure of 1 bar.
†α = percent of Fe reacted/100 (*e.g.*, $\alpha = 0.0041$ for run H221).

TABLE 4. Experimental data for the oxidation of Gibeon filings.*

Run number	Temp. (°C)	Time (h)	w_i (mg)	$100 \times \Delta w/w_i$ (%)	Fe reacted† (%)
H241	179	528	75.35	0.77	2.02
H237	230	44.5	90.06	1.30	3.42
H236	281	44.5	113.89	1.89	4.94
H217	335	44.5	73.26	7.24	18.95
H216	390	44.5	59.77	14.34	37.54
H215	442	44.5	116.11	23.70	62.04

*H_2/H_2O is 4.1, total pressure of 1 bar.
†α = percent of Fe reacted/100 (*e.g.*, $\alpha = 0.0202$ for run H241).

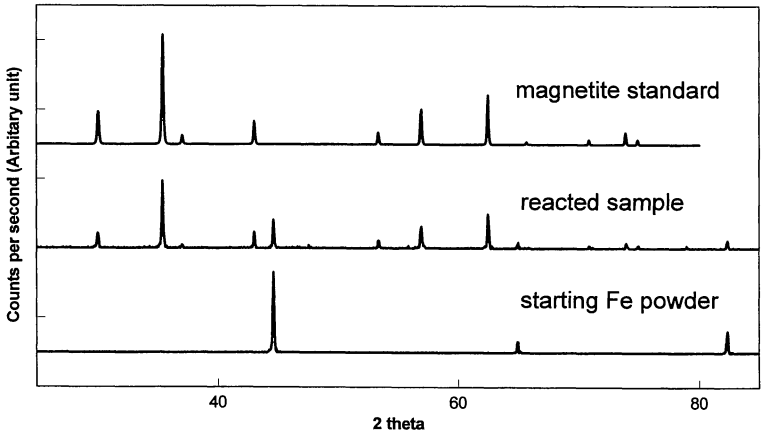

FIG. 4. X-ray diffraction patterns of the starting Fe powder, a reacted sample, and the magnetite standard. The XRD pattern of the reacted sample shows reflections from magnetite and residual Fe metal.

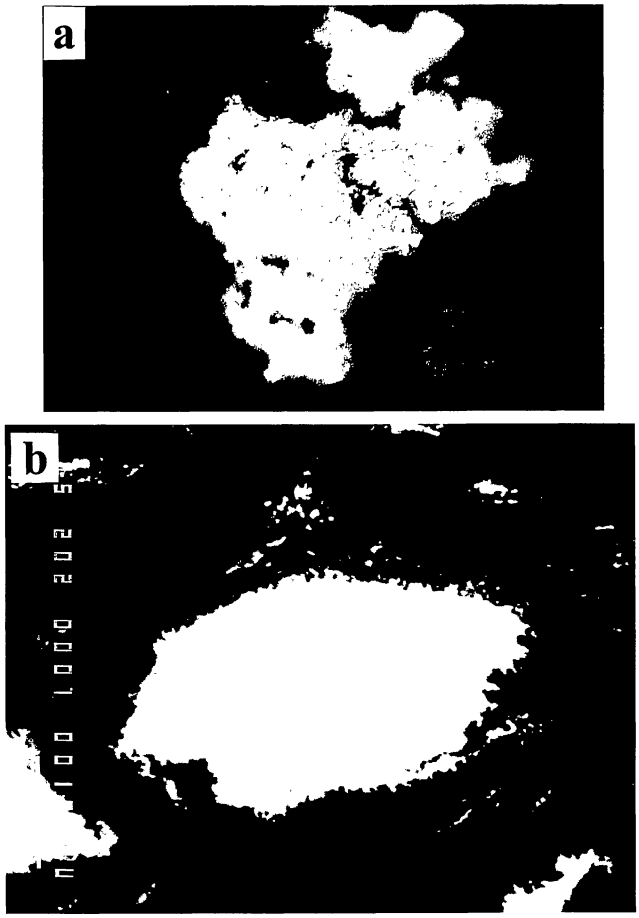

FIG. 5. (a) Reflected light optical micrograph of the cross-section of a partially reacted Fe powder ($H_2/H_2O \sim 4.1$ gas mixture at 390 °C for 140 h). The gray areas are magnetite and the bright areas are remnant Fe metal. The scale bar to the left is 10 μm. (b) Scanning electron microscope image of the cross-section of partially reacted Gibeon metal filings ($H_2/H_2O \sim 4.1$ gas mixture at 442 °C for 44.5 h). The gray rim (~2 μm) surrounding the metal is magnetite. The scale bar is 10 μm.

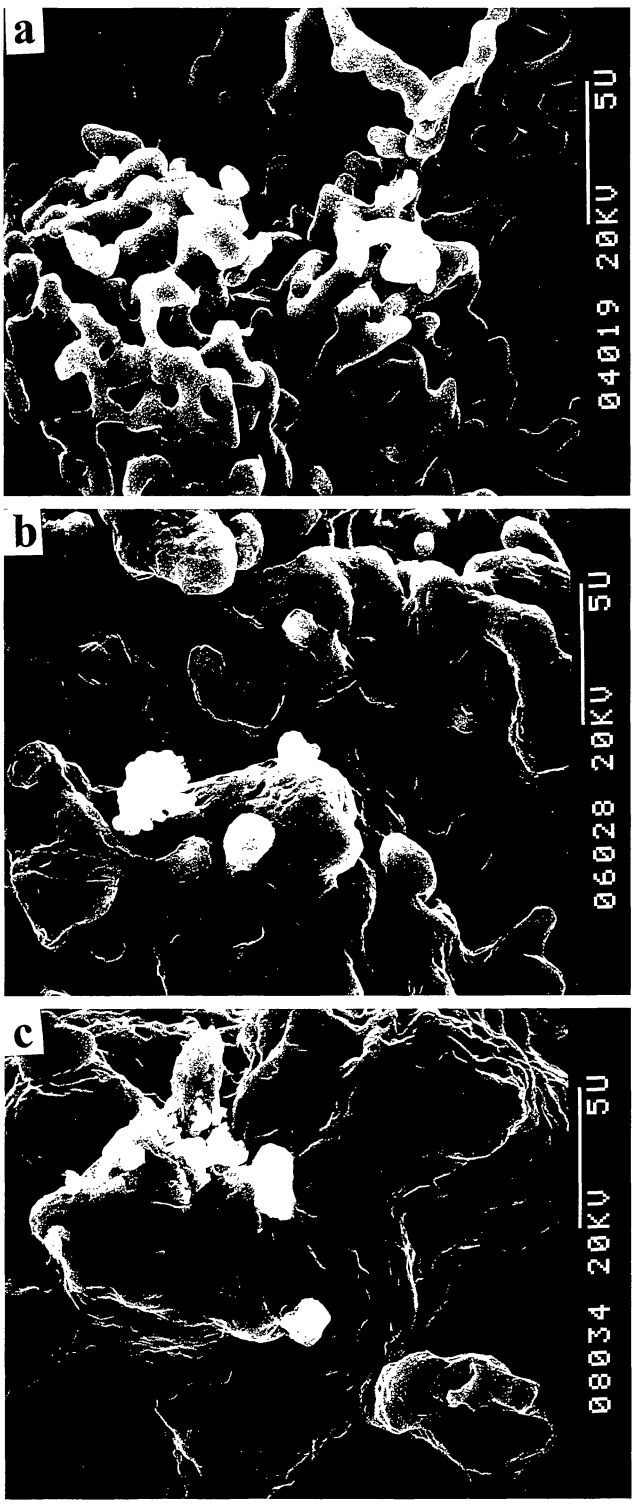

FIG. 6. Scanning electron microscope images of reacted Fe powder after different extents of reaction: (a) 4.81%, (b) 36.28%, and (c) 48.27%. The void space in the reacted sample decreases as the extent of reaction increases due to the increased molar volume of magnetite in the product.

Fe_3O_4). The powder is a network of "wormy" Fe metal with extensive porosity. As the reaction proceeds, the porosity decreases, the surface of the Fe metal becomes coated with a rougher layer of magnetite, and the oxide grows to fill the void spaces. The void spaces are filled by magnetite because Fe_3O_4 has a much larger molar volume than Fe (44.52 $cm^3\ mol^{-1}$ *vs.* 7.09 $cm^3\ mol^{-1}$, respectively). Figure 6b (36.3% conversion) and Fig. 6c (48.3% conversion) illustrate this trend with increasing extent of reaction. These observations are consistent with the specific surface area measurements and derived sizes of the initial Fe powder and reacted samples, which are summarized in Table 5.

The BET surface area measurements give an estimate of the particle size that is called the equivalent spherical diameter. This is defined as

$$D = \frac{6}{S \times \rho} \tag{8}$$

where D, in micrometers, is the equivalent spherical diameter; S, in $m^2\ g^{-1}$, is the specific surface area of the sample; and ρ, in g cm^{-3}, is the density of the starting material or the reacted sample. The equivalent spherical diameters of the powders and Gibeon metal filings (see Table 5) are significantly smaller than the particle sizes determined from microscopy. This difference arises because of the high porosity of the Fe powders and the roughness of the Gibeon metal filings.

TABLE 5. Surface areas and sizes of iron metal powder and Gibeon metal filings.

Sample	Extent of Reaction† (%)	Sp. surf. area‡ (m^2/g)	Equiv. spherical diameter (μm)§
Iron powder*	0	0.65	1.2
H235	0.88	–	–
H226	4.81	0.60	1.3
H227	10.03	0.61	1.3
H222	36.28	0.47	1.6
H224	68.91	0.32	2.4
Gibeon filings*	0	3.41	0.23
H241	2.02	2.71	0.28
H237	3.42	2.77	0.28
H236	4.94	2.03	0.38
H217	18.95	1.82	0.42
H216	37.54	1.67	0.46

*Iron powder and Gibeon filings before annealing.
†From Table 3.
‡From N_2 gas absorption measurements.
§Calculated from equation (8) in the text.

Two effects decrease the surface area of the starting Fe powders and Gibeon metal filings. The metal powders sinter somewhat during annealing at 450 °C, a temperature higher than that for the subsequent reactions. Second, magnetite growth on the powders and filings during reaction also decreases the specific surface areas of the reacted samples (*e.g.*, from 0.6 to 0.3 $m^2\ g^{-1}$ for the Fe powder and from 2.7 to 1.7 $m^2\ g^{-1}$ for the Gibeon filings) as magnetite fills up pores in the Fe powder and covers the rough surface of the Gibeon metal filings. The decreased surface area due to magnetite formation can be incorporated into the kinetic modeling (see below).

Rate of Magnetite Formation

Gas–solid reactions follow different rate laws depending upon the type of solid, temperature and time period of reaction, reactive gas partial pressure, and rate controlling mechanism (Brown *et al.*, 1980). We used the weight gain data and the BET surface area data from our experiments to determine the magnetite formation rate and type of rate law followed.

Linear or Parabolic Kinetics–Linear and parabolic rate laws can be distinguished by plotting the reaction progress *vs.* time. Depending on whether metal foils or powders are being studied, it is convenient to define the reaction progress as the weight gain per square centimeter surface area ($\Delta w/A$), the fractional weight gain ($\Delta w/w_i$), or as the fraction reacted (α). Here we use the fraction of metal reacted (α), which is given by the following equation:

$$\alpha = \frac{\Delta w}{w_i} \times f_{st} \tag{9}$$

where Δw is the weight gain of the powder (or filings), w_i is the initial weight of the powder (or filings), and f_{st} is a stoichiometric factor derived from the mass balance in reaction (1). The value of f_{st} = 2.6179, and this factor converts the measured weight gain (Δw) of the sample to the weight of Fe oxidized to Fe_3O_4. As discussed later, the magnetite formed from the Gibeon meteorite metal filings contains a small amount of NiO and CoO, which makes f_{st} ~0.1% larger than the value for pure magnetite. This small increase in f_{st} was neglected and 2.6179 was used for calculating α for pure Fe metal and Gibeon meteorite metal.

If the oxidation or corrosion rate of metals is limited by the supply of gas molecules, adsorption, or the rate of chemical reaction at the gas–solid interface, then linear kinetics are followed and the plot of reaction progress *vs.* time (t) gives a straight line

$$\alpha = \frac{\Delta w}{w_i} \times f_{st} = k_l t \tag{10}$$

with a slope k_l equal to the linear rate constant of the reaction. For example, Lauretta *et al.* (1996a,b) observed that Fe metal corrosion by H_2S initially follows linear kinetics, especially at low H_2S concentrations. The linear rate constant can have units such as h^{-1}, g cm^{-2} h^{-1} or cm h^{-1} depending on how the reaction progress has been defined.

Once diffusion (*e.g.*, of Fe) through the product layer becomes rate limiting, parabolic kinetics are followed and the plot of reaction progress *vs.* time is no longer linear with time, but instead reaction progress squared is proportional to time:

$$\alpha^2 = \left[\frac{\Delta w}{w_i} \times f_{st}\right]^2 = k_p t \tag{11}$$

where k_p is the parabolic rate constant, which is calculated from the slope of the plot of reaction progress squared *vs.* time and can have units of h^{-1}, $g^2\ cm^{-4}\ h^{-1}$, or $cm^2\ h^{-1}$, depending on how the reaction progress has been defined.

The experimental data for the oxidation of Fe powder and Gibeon meteorite metal filings in the H_2/H_2O ~ 4.1 gas mixture are listed in Tables 3 and 4. The fraction of Fe oxidized to magnetite at several different temperatures is plotted *vs.* the square root of reaction time in Fig. 7. This is mathematically equivalent to equation (11) but is perhaps more easily understood. The straight line plots show that Fe oxidation follows parabolic kinetics under our experimental conditions and that diffusion of the reactants in the magnetite layer is the rate-limiting step. By analogy with iron sulfide formation on Fe metal in H_2S-H_2 gas mixtures (Lauretta *et al.*, 1996a,b), the outward diffusion of Fe ions is plausibly the rate-limiting step for magnetite formation in our experiments. The data do not follow linear kinetics, which was also tested in our data analysis. Other groups have also found that magnetite formation from Fe metal or Fe-Ni alloys below the wüstite eutectoid temperature (~570 °C) follows parabolic kinetics instead of linear kinetics (Seo and Sato, 1983; Gemma *et al.*, 1990).

Rate Constants and Activation Energy–We calculated the rate constant and activation energy for magnetite formation using the constant area, Jander, Ginstling–Brounshtein, and Valensi–Carter models (Hulbert, 1969; Brown *et al.*, 1980). All four methods model magnetite formation from Fe powder and Gibeon metal filings as the reaction of spherical metal particles with uniform radii equal to that calculated from the BET surface area measurements using equation (8). This assumption is reasonable because the gas adsorption surface area is the reactive surface area of the porous, irregularly shaped metal particles. Hulbert (1969) notes that the Jander, Ginstling–Brounshtein, and Valensi–Carter models represent the kinetics of many actual powder reactions.

The constant area model is the simplest model because it neglects the decrease in the surface area (A) of the Fe powder during magnetite formation. The rate constant is given by:

$$k_p = \left[\frac{\Delta w \times f_{st}}{A \times t \times \rho_{Fe}}\right]^2 \text{cm}^2\text{h}^{-1} \tag{12}$$

where ρ_{Fe} is the density of Fe metal (7.9 g cm^{-3}), and the other terms have already been defined. We used BET surface areas of 0.60 $m^2\ g^{-1}$ and 2.7 $m^2\ g^{-1}$ for Fe metal powder and Gibeon metal

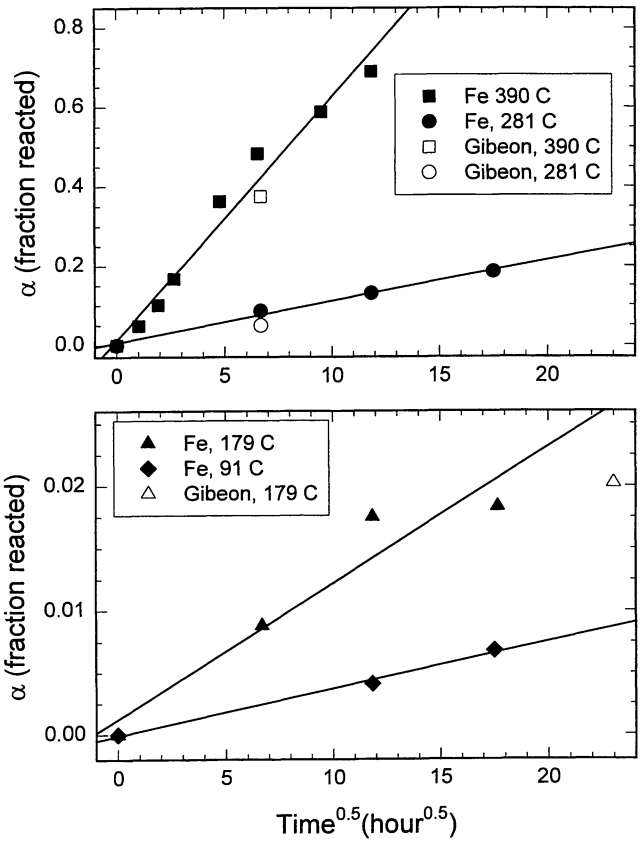

FIG. 7. The fraction of Fe metal oxidized to magnetite at four different temperatures. The error bars are less than the size of the experimental points. The linear regression for conversion *vs.* time$^{1/2}$ shows parabolic kinetics, which means that diffusion (*e.g.*, of Fe) through the magnetite layer is the rate-limiting step.

filings, respectively, for evaluating equation (12). These surface areas are representative of the metal powder and filings after annealing, which causes a small decrease in the reactive surface area of the Fe powder and Gibeon filings (data for samples H226 and H241).

The Jander model was originally developed by applying the parabolic rate law to powders (see Hulbert, 1969). Later workers have improved on Jander's model by considering the decrease in reactive surface area as the reaction proceeds (the Ginstling–Brounshtein equation) and the different molar volumes of the product and reactant (the Valensi–Carter equation), which is

$$k_p = \frac{r_o^2}{t}\left[\frac{Z-(Z-1)(1-\alpha)^{\frac{2}{3}}-(1+(Z-1)\alpha)^{\frac{2}{3}}}{(Z-1)}\right] \text{cm}^2\text{h}^{-1} \qquad (13)$$

In equation (13), r_o is the initial particle radius, t is time, α is the fraction reacted, and Z is volume of product formed per unit volume of reactant consumed, which is equal to 2.093 for magnetite formation from Fe metal.

Table 6 summarizes our calculations and shows that similar rate constants and activation energies are computed from the four models. For example, activation energies of 92, 95, 94, and 92 kJ mol^{-1} are calculated for magnetite formation from Fe metal using the constant area, Jander, Ginstling–Brounshtein, and Valensi–Carter models, respectively. We use the rate constants and activation energies from the Valensi–Carter model because it is the most realistic of the four

TABLE 6. Kinetic data for iron powder and Gibeon filings.

Model	$\log_{10} k$ (cm^2 h^{-1})	E_{act} (kJ mol^{-1})
Iron Powder		
Constant area	–4.54 (±0.26) – 4799 (±254)/T	92 ± 5
Jander	–4.12 (±0.34) – 4984 (±330)/T	95 ± 6
Ginstling–Brounshtein	–4.26 (±0.30) – 4919 (±296)/T	94 ± 6
Valensi–Carter	–4.14 (±0.26) – 4825 (±260)/T	92 ± 5
Gibeon Filings		
Constant area	–5.81 (±0.44) – 4902 (±652)/T	94 ± 12
Jander	–5.26 (±0.44) – 5169 (±656)/T	99 ± 13
Ginstling–Brounshtein	–5.45 (±0.44) – 5075 (±650)/T	97 ± 12
Valensi–Carter	–5.41 (±0.44) – 4942 (±646)/T	95 ± 12

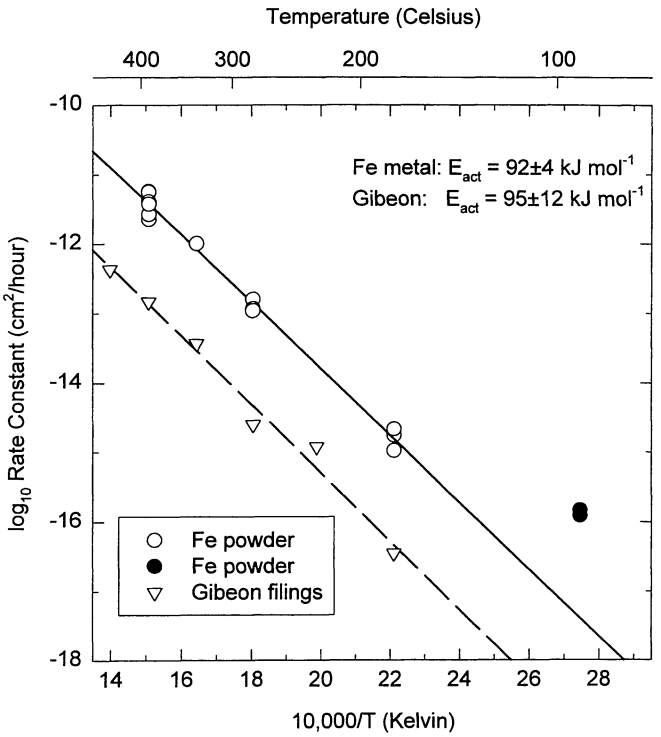

FIG. 8. An Arrhenius plot of the reaction rate constants for oxidation of Fe powder and Gibeon metal filings to magnetite. The slopes of the lines give the activation energies. The error bars are less than the size of the experimental points. The points at 91 °C (black dots) are not included in the linear least-squares fits for reasons discussed in the text.

models (*e.g.*, both the decrease in reactive surface area of the metal and the different molar volumes of the metal and oxide are considered).

Figure 8 is an Arrhenius plot of $\log_{10} k_p$ (cm^2 h^{-1}) *vs.* 10 000/T for the Fe and Gibeon metal. Good linear least-squares fits are obtained for all the kinetic data, except for the Fe metal points at 91 °C. This discrepancy is discussed below. The equations for the linear least-squares regression lines are

$$\log_{10} k_p = -4.14\ (\pm 0.26) - \frac{4825(\pm 260)}{T}\ \text{cm}^2\ \text{h}^{-1} \qquad (14)$$

for the pure Fe powder and

$$\log_{10} k_p = -5.41\ (\pm 0.44) - \frac{4942(\pm 646)}{T}\ \text{cm}^2\ \text{h}^{-1} \qquad (15)$$

for the Gibeon metal filings. In both equations, the temperature T is in Kelvins. Equations (14) and (15) are our derived equations for the rate constants of magnetite formation from Fe metal and Gibeon meteorite metal. The parabolic rate constant for Fe metal is ~28× larger than that for Gibeon metal filings under our experimental conditions. This difference is probably related to the Ni content of the Gibeon metal, but more work is needed to define the effects of minor and trace constituents in meteoritic metal such as Ni, Co, and P on magnetite formation.

The high reaction rate of the Fe powder oxidized at 91 °C is also of interest. This could indicate that the magnetite layer is growing by a different reaction mechanism at lower temperatures, for example, *via* grain boundary diffusion instead of bulk diffusion. This suggestion is consistent with experimental studies showing that the parabolic rate constant for magnetite formation below 570 °C is up to two orders of magnitude larger than predicted from calculations using high temperature Fe^{2+} bulk diffusion coefficients in magnetite (Tinkler and Dieckmann, 1992). Lauretta *et al.* (1996a,b) observed that FeS formation from pure Fe at low temperatures was faster than predicted from the Arrhenius plot of the higher temperature rate data. In this case, crystallographically oriented FeS crystals grow rapidly at low temperatures because of rapid Fe^{2+} diffusion along the *a* axis of the sulfide crystals. Further work is needed to study magnetite formation at and below 100 °C in more detail.

Comparison of Magnetite and Iron Sulfide Formation Rates–As mentioned earlier, our preliminary experiments with Fe metal foils and Gibeon meteorite pieces did not give useful kinetic data. In contrast, our earlier experiments on iron sulfide formation produced thick sulfide layers and provided useful kinetic data (Lauretta *et al.*, 1996b). In hindsight using equation (14), it is easy to see why iron sulfide formation is relatively easy to study whereas magnetite formation is more difficult. Lauretta *et al.* (1996b) observed formation of iron sulfide layers ~34 μm thick after 48 h at 673 K in a 850 ppmv H_2S/H_2 gas mixture (their Fig. 3). Growth of this iron sulfide layer followed parabolic kinetics, and the parabolic rate constant (k_p) is ~2.4 × 10^{-7} cm^2 h^{-1}. In contrast, equation (14) predicts k_p ~ 4.9 × 10^{-12} cm^2 h^{-1} for magnetite formation in a H_2/H_2O ~ 4.1 gas mixture at the same temperature. After the same time (48 h), the magnetite layer would be only ~0.15 μm thick. Furthermore, because the layer thickness is proportional to the square root of time, the formation of thicker layers requires extremely long times: a 1.5 μm thick magnetite layer requires ~191 days reaction at 673 K in the same gas mixture.

These comparisons also indicate that magnetite formation in the solar nebula will be much slower than FeS formation. We consider this question after discussing the Ni and Co in the magnetite layers on Gibeon meteorite metal.

Nickel and Cobalt Concentrations

We analyzed the Ni and Co concentrations in the starting Gibeon filings, in the remnant Gibeon metal after reaction, and in the magnetite product by electron microprobe. The results are expressed as cation wt% (*e.g.*, cation wt% Ni = 100 × [Ni/(Fe + Ni + Co)]) to compare changes between the Ni and Co contents of metal and oxide and are shown in Figs. 9 and 10.

Figure 9 shows the results of electron microprobe analyses of the Ni concentrations in the starting Gibeon metal, remnant metal, and the oxide product. A broad beam focus (~20 μm) was used for analyses of the starting metal. A narrow beam focus (~1 μm in diameter) was used for analyses of the remnant metal and magnetite product.

The broad beam analysis of the starting Gibeon metal showed ~7 wt % Ni in the large kamacite areas, with Ni concentrations up to 21 wt% in the kamacite–taenite bands or spots. The average Ni content in the starting Gibeon is 8.4 wt% (with 7.0 wt% being the central value in the histogram in Fig. 9a). After the reaction, the average Ni content changed to 7.3 wt% in the remnant metal (Fig. 9b), and the average Ni concentration in the oxide product was 3.3 wt% (Fig. 9c).

The same trend was observed for Co, as shown in Fig. 10. The starting Gibeon metal has a smoother Co concentration distribution centered at 0.44 wt% (average of 60 analyses). Cobalt is depleted in the oxide product (0.24 wt%) and enriched in the remnant metal (0.52 wt%) relative to its concentration in the initial Gibeon meteorite metal.

The ratios of Fe/Ni, Fe/Co, and Ni/Co are different in the starting metal, in the remnant metal, and in the oxide. The different ratios suggest that Ni and Co in the starting alloy were also oxidized and that the Ni and Co in the oxide layer are present as oxides and not as small remnant metal grains. Thermodynamic calculations of the oxidation of Fe-Ni-Co alloy (Gibeon metal, 91.1 wt% Fe, 8.4 wt% Ni, 0.4 wt% Co) were made to predict the Ni and Co content in the oxide. The thermodynamically stable Ni- and Co-bearing oxides under our experimental conditions are $NiFe_2O_4$ and $CoFe_2O_4$ (Robie and Hemingway, 1995; Kubaschewski *et al.*, 1993), and the amounts of Ni and Co that are in oxide can be calculated from the following reactions:

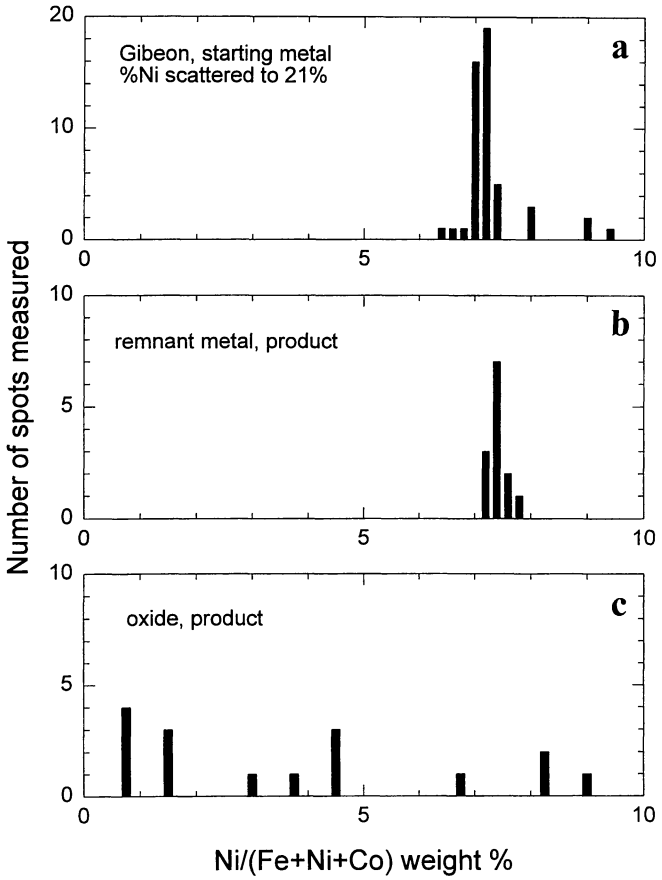

FIG. 9. Histograms showing the Ni concentrations (wt%) in the starting Gibeon meteorite metal, the remnant metal, and the magnetite layer. The histograms show that Ni is depleted in the oxide layer and enriched in the remnant metal.

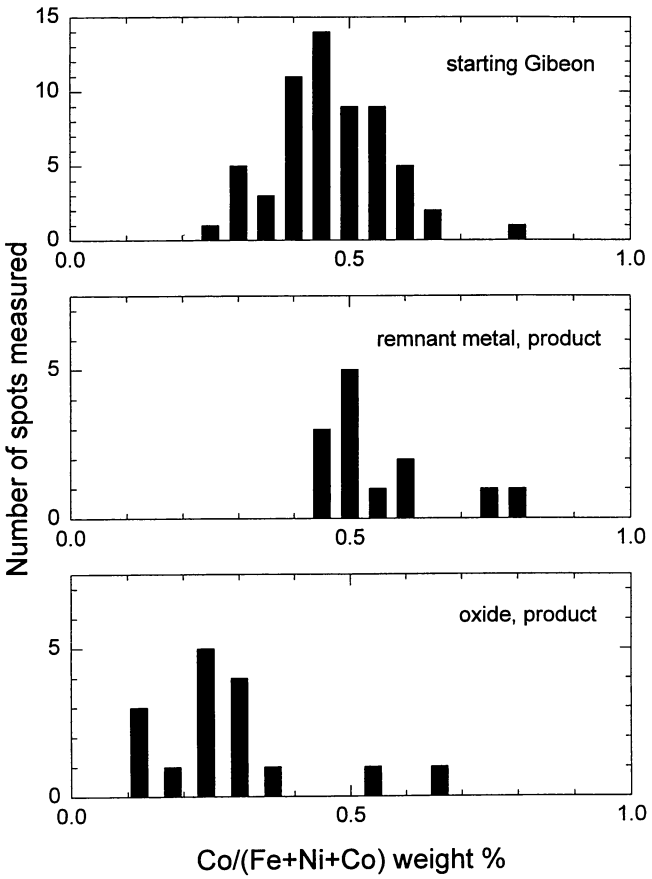

FIG. 10. Histograms showing the Co concentrations (wt%) in the starting Gibeon meteorite metal, the remnant metal, and the magnetite layer. The histograms show that Co is depleted in the oxide layer and enriched in the remnant metal.

$$Ni\ (alloy) + Fe_3O_4\ (magnetite) = NiFe_2O_4\ (trevorite) + Fe\ (alloy) \quad (16)$$

$$Co\ (alloy) + Fe_3O_4\ (magnetite) = CoFe_2O_4\ (Co,Fe\ oxide) + Fe\ (alloy) \quad (17)$$

Using thermodynamic data for Fe_3O_4 and $NiFe_2O_4$ from Robie and Hemingway (1995), and data for $CoFe_2O_4$ from Kubaschewski *et al.* (1993), and assuming ideal solid solutions in the metal and oxide (Kubaschewski *et al.*, 1993; Katayama *et al.*, 1979), the mole fractions of $NiFe_2O_4$ and $CoFe_2O_4$ in the oxide are 1.03×10^{-5} and $\sim 1.07 \times 10^{-7}$ (Ni and Co cation wt% of 3.4×10^{-4} and 3.6×10^{-6}, respectively) at 700 K. This means that Ni and Co will be depleted in the oxide and enriched in the remnant metal, which is the trend observed in our experiments. However, the observed Ni and Co concentrations in the oxide are much higher than the predicted values. This disequilibrium phenomenon of much higher Ni and Co concentrations is perhaps due to kinetic factors, and a similar effect was also observed in Fe-Ni alloy oxidation in CO_2 at 700–1000 °C (Menzies and Tomlinson, 1966; Tomlinson and Menzies, 1978). They found that Ni concentrations are higher than the predicted equilibrium levels in the oxide during the initial stage of oxidation. They also observed that the Ni concentration in the oxide decreases gradually with time as oxidation proceeds.

MAGNETITE FORMATION TIME IN THE SOLAR NEBULA

We now use our kinetic data to calculate the time required to convert Fe alloy particles to magnetite by vapor phase oxidation in the solar nebula. The lifetime (t_{100}) for complete oxidation of spherical metal grains with uniform radii (r in micrometers) is given by

$$t_{100} = \frac{(10^{-4} r)^2}{k_p} \times 1.14 \times 10^{-4}\ \text{years} \quad (18)$$

where k_p is taken from equations (14) and (15) for pure Fe and Gibeon metal. The percentage of Fe metal reacted at any time t is given by

$$\% = 100 \times \sqrt{\frac{t}{t_{100}}} \quad (19)$$

because magnetite growth follows parabolic kinetics.

We checked equations (18) and (19) against our results at 179 °C, the lowest temperature used to calculate the rate constant equations for pure Fe and Gibeon. The predicted and observed values are in satisfactory agreement: 0.40% *vs.* 0.88% at 44.5 h, 0.70% *vs.* 1.75% at 140 h, and 1.06% *vs.* 1.83% at 312 h for pure Fe (0.65 μm radius grains). We also calculated 1.1% *vs.* 2.0% reacted for Gibeon after 528 h at 179 °C (0.14 μm radius grains).

The results of the metal grain lifetime calculations are given in Table 7. The lifetimes of small metal grains (0.1 μm radius) are well within the 0.1–10 Ma estimated lifetime of the solar nebula (Podosek and Cassen, 1994) over all temperatures considered for magnetite formation (350–400 K). The lifetimes of 1 μm radius metal grains are 100× longer at a given temperature but still generally fall within 10 Ma. However, the times required for complete oxidation of 10 μm radius metal grains exceed the 10 Ma estimated nebular lifetime at and below 375 K. This is just 10° below the magnetite formation temperature (if all C is in CH_4), but it is 18° higher than the magnetite formation temperature if all C remains as CO.

Equation (19) indicates that some grains, which cannot be completely converted to magnetite (*e.g.*, because they are too large or because they aggregate and are removed from reaction with nebular gas), may still be partially oxidized. Thus, many metal grains could be covered with magnetite rims of varying thickness. To take an extreme case, Table 7 gives lifetimes of 10^8 to 4×10^9 years for 10 μm radius metal grains at 350 K. Taking the nebular lifetime as 10^7 years and applying equation (19), it is possible that 32% to 5% of the metal could be oxidized to magnetite (if the metal grain does not grow in size and it remains in contact with the nebular gas for all this time). Likewise, smaller grains may be partially rimmed by magnetite before they agglomerate with one another to form larger grains, which then cease reacting.

However, the calculated lifetimes for Fe alloy oxidation in the nebula may be lower limits because our rate equations are based on experiments done in fairly water-rich H_2/H_2O gas mixtures containing

TABLE 7. Lifetime for iron alloy grains (years).*

T (K)	0.1 μm*	1 μm*	10 μm*
400	$2 \times 10^2 - 7 \times 10^3$	$2 \times 10^4 - 7 \times 10^5$	$2 \times 10^6 - 7 \times 10^7$
375	$1 \times 10^3 - 4 \times 10^4$	$1 \times 10^5 - 4 \times 10^6$	$1 \times 10^7 - 4 \times 10^8$
350	$1 \times 10^4 - 4 \times 10^5$	$1 \times 10^6 - 4 \times 10^7$	$1 \times 10^8 - 4 \times 10^9$

*Grain radii are listed.

200–450× more water than expected in the solar nebula. By analogy with iron sulfide formation in H_2/H_2S gas mixtures (Lauretta *et al.*, 1996a), we expect that the magnetite formation rate will decrease as the H_2/H_2O ratio increases (*i.e.*, the Fe alloy grain lifetimes for oxidation will increase). It is also possible that at sufficiently low pressures, the magnetite formation rate could be limited by collisions of H_2O molecules on the surface of the metal grains, as assumed in the SCT models. On the other hand, low-temperature (<400 K) oxidation may proceed faster than predicted from extrapolation from higher temperatures because of short circuit diffusion pathways (Tinkler and Dieckmann, 1992).

SUMMARY

Our experiments show formation of magnetite from Fe metal or iron meteorite metal at 91–442 °C at ambient atmospheric pressure (~1 bar) in an He (87.8%) – H_2 (9.8%) – H_2O (2.4%) gas mixture with an H_2/H_2O molar ratio ~ 4.1, and at 100–235 °C in an H_2 (97.6%) – H_2O (2.4%) gas mixture with an H_2/H_2O molar ratio ~ 41. Our experiments also show that without H_2O in the H_2-He gas mixture, magnetite is reduced back to Fe metal. These observations are consistent with the Fe-O phase diagram in Fig. 1.

We obtained kinetic data in the H_2/H_2O ~ 4.1 gas mixture at temperatures of 179–442 °C for pure Fe powder and Gibeon meteorite metal filings. Parabolic kinetics were observed, and the activation energy is ~92 kJ/mol in both cases. Larger rate constants were observed at a given temperature in this temperature range for pure Fe than for Gibeon metal. The magnetite formation rate constants are significantly smaller than the parabolic rate constants for iron sulfide formation from Fe in the same temperature range.

Finally, the lifetimes of small Fe alloy particles were calculated at temperatures in the magnetite stability field below 400 K. The results, which are listed in Table 7, show that the lifetimes of 0.1–1 μm radius metal grains are generally within the estimated lifetime of the solar nebula. These lifetimes are best regarded as lower limits, and magnetite formation in the nebula may take much more time if (as expected) the oxidation rate decreases as the H_2/H_2O ratio of the gas mixture increases. However, there are more parameters that need to be investigated, for example, large H_2/H_2O ratios, low temperatures below 400 K, lower total pressures, and metal alloy composition in order to get a thorough understanding of magnetite formation from Fe alloy in the solar nebula. These studies are currently underway in our laboratory.

Acknowledgments–This work was supported by NASA grant NAG5-4323, formerly NAGW-3070. We thank Dr. K. Lodders and Dr. D. Lauretta for helpful discussions; Ms R. Osborne for measuring the particle size; Dr. D. Kremser and Mr. R. Poli for technical assistance. We thank R. Hewins and an anonymous referee for helpful reviews and the editor H. Nagahara for her comments.

Editorial handling: H. Nagahara

REFERENCES

ANDERS E. (1971) Meteorites and the early solar system. *Ann. Rev. Astron. Astrophys.* **9,** 1–34.

ANDERS E. (1972) Physico-chemical processes in the solar nebula, as inferred from meteorites. In *Symposium on the Origin of the Solar System* (ed. H. Reeves), pp. 179–201. CNRS, Paris, France.

BOSTRÖM K. AND FREDRIKSSON K. (1966) *Surface Condition of the Orgueil Meteorite Parent Body as Indicated by Mineral Associations.* Smithsonian Misc. Coll. **151,** Smithsonian Institution, Washington, D.C., USA. 39 pp.

BRADLEY J. P., BROWNLEE D. E. AND FRAUNDORF P. (1984) Carbon compounds in interplanetary dust: Evidence for formation by heterogeneous catalysis. *Science* **223,** 56–58.

BROWN M. E., DOLLIMORE D. AND GALWEY A. K. (1980) Theory of solid state reaction kinetics. In *Comprehensive Chemical Kinetics,* vol. 22 (eds. C. H. Bamford and C. F. H. Tipper), pp. 41–113. Elsevier, Amsterdam, The Netherlands.

CHOI B. G., MCKEEGAN K. D., LESHIN L. A. AND WASSON J. T. (1997) Origin of magnetite in oxidized CV Chondrite: In situ measurement of oxygen isotope composition of Allende magnetite and olivine. *Earth Planet. Sci. Lett.* **146,** 337–349.

DUFRESNE E. R. AND ANDERS E. (1962) On the chemical evolution of the carbonaceous chondrites. *Geochim. Cosmochim. Acta* **26** 1085–1114.

FEGLEY B., JR. (1988) *Cosmochemical trends of volatile elements in the solar system.* LPI Technical Report **88–04,** 51–60.

FEGLEY B., JR. (1993) Chemistry of the solar nebula. In *The Chemistry of Life's Origins* (eds. M. Greenberg, C. X. Mendoza-Gomez and V. Pirronello), pp. 75–147. NATO Advanced Science Institute, Series C vol. 416, Kluwer Academic Publishers, Dordrecht, The Netherlands,.

FEGLEY B., JR. AND PRINN R. G. (1989) Solar nebula chemistry: Implications for volatiles in the solar system. In *The Formation and Evolution of Planetary Systems* (eds. H. A. Weaver and L. Danly), pp. 171–211. Cambridge Univ. Press, Cambridge, U.K.

GEMMA K., KAWAKAMI M., KOBAYASHI C., ITOH N. AND TOMIDA M. (1990) Kinetics of oxidation of pure iron near the eutectoid temperature of wüstite. *J. Mater. Sci.* **25,** 4555–4561.

GREGG S. J. AND SING K. S. W. (1982) *Adsorption, Surface Area and Porosity.* Academic Press, New York, New York, USA. 371 pp.

GREVESSE N. AND NOELS A. (1993) Cosmic abundances of the elements. In *Origin and Evolution of the Elements* (eds. N. Prantzos, E. Vangioni-Flam and M. Cassé), pp. 15–25. Cambridge Univ. Press, Cambridge, U.K.

GROSSMAN L. (1972) Condensation in the primitive solar nebula. *Geochim. Cosmochim. Acta* **36,** 597–619.

HULBERT S. F. (1969) Models for solid-state reactions in powdered compacts: A review. *J. Br. Ceram. Soc.* **6,** 11–20.

HYMAN M. AND ROWE M. W. (1983) Magnetite in CI chondrites. *J. Geophys. Res.* **88,** 736–740.

JEDWAB J. (1967) La magnetite en plaquettes des meteorites carbonees D'alais, Ivuna et Orgueil. *Earth Planet. Sci. Lett.* **2,** 440–444.

JEDWAB J. (1971) La magnétite de la météorite D'Orgueil Vue au microscope electronique a Balayage. *Icarus* **15,** 319–340.

KATAYAMA I., WATANABE Y. AND KOZUKA I. (1979) Thermodynamic study of spinel type solid solutions of the Fe_3O_4–$NiFe_2O_4$ system by the EMF method. *Trans. Jap. Inst. Met.* **20,** 593–596.

KERRIDGE J .F. (1970) Some observations on the nature of magnetite in the Orgueil meteorite. *Earth Planet. Sci. Lett.* **9,** 299–306.

KERRIDGE J. F., MACKAY A. L. AND BOYNTON W. V. (1979) Magnetite in CI carbonaceous meteorites: Origin by aqueous activity on a planetesimal surface. *Science* **205,** 395–397.

KROT A. N., SCOTT E. R. D. AND ZOLENSKY M. E. (1995) Mineralogical and chemical modification of components in CV3 chondrites: Nebular or asteroidal processing? *Meteoritics*, **30,** 748–775.

KROT A. N., ZOLENSKY M. E., WASSON J. T., SCOTT E. R. D., KEIL K. AND OHSUMI K. (1997) Carbide-magnetite assemblages in type-3 ordinary chondrite. *Geochim. Cosmochim. Acta* **61,** 219–237.

KUBASCHEWSKI O. AND HOPKINS B. E. (1953) *Oxidation of Metals and Alloys.* Butterworth-Heinemann, London, U.K. 239 pp.

KUBASCHEWSKI O., ALCOCK C. B. AND SPENCER P. J. (1993) *Materials Thermochemistry*, 6th ed. Pergamon Press, Oxford, U.K. 363 pp.

LARIMER J. W. (1967) Chemical fractionation in meteorites–I. Condensation of the elements. *Geochim. Cosmochim. Acta* **31,** 1215–1238.

LAURETTA D. S. (1997) Theoretical and experimental studies of iron-nickel-sulfur, beryllium, and boron cosmochemistry. Ph.D. thesis, Washington University, St. Louis, Missouri, USA. 455 pp.

LAURETTA D. S., KREMSER D. T. AND FEGLEY B., JR. (1996a) The rate of iron sulfide formation in the solar nebula. *Icarus* **122,** 288–315.

LAURETTA D. S., FEGLEY B., JR., LODDERS K. AND KREMSER D. T. (1996b) The kinetics and mechanism of iron sulfide formation in the solar nebula. *Proc. NIPR Symp. Antarct. Meteorites* **9,** 111–126.

LAURETTA D. S., LODDERS K. AND FEGLEY B., JR. (1997) Experimental simulations of sulfide formation in the solar nebula. *Science* **277,** 358–360.

LEWIS J. S. AND PRINN R. G. (1980) Kinetic inhibition of CO and N_2 reduction in the solar nebula. *Astrophys. J.* **238,** 357–364.

LIDE D. R. (1996) *CRC Handbook of Chemistry and Physics*, 77th ed. CRC Press, Cleveland, Ohio, USA. 2477 pp.

MELVILLE H. AND GOWENLOCK B. G. (1964) *Experimental Methods in Gas Reactions.* MacMillan & Co., New York, New York, USA. 389 pp.

MENZIES I. A. AND TOMLINSON W. J. (1966) Oxidation of an Fe-2.29% Ni alloy in carbon dioxide at 600–1000 °C. *J. Iron Steel Inst.* **204,** 1239–1252.

NAGAHARA H. (1984) Matrices of type 3 ordinary chondrites—primitive nebular records. *Geochim. Cosmochim. Acta* **48,** 2581–2595.

PODOSEK F. A. AND CASSEN P. (1994) Theoretical, observational, and isotopic estimates of the lifetime of the solar nebula. *Meteoritics* **29,** 6–25.

ROBIE R. A. AND HEMINGWAY B. S. (1995) *Thermodynamic Properties of Minerals and Related Substances at 298.15 K and 1 Bar (105 Pascals) Pressure and at Higher Temperatures.* USGS Bull. 2131, Washington, D.C., USA. 456 pp.

SEO M. AND SATO N. (1983) Selective oxidation of Fe-30Ni alloy in a low-temperature range (433–473 K). *Oxid. Met.* **19,** 151–163.

TINKLER S. AND DIECKMANN R. (1992) Limited role of cation bulk diffusion in the oxidation of pure iron to magnetite. *J. Mater. Sci.* **27,** 3799–3802.

TOMLINSON W. J. AND MENZIES I. A. (1978) Oxidation of an Fe-19 wt. % Ni alloy in CO_2 at 700–1000 °C. *Oxid. Metals* **12(3),** 215–225.

TURKDOGAN E. T., MCKEWAN W. M. AND ZWELL L. (1965) Rate of oxidation of iron to wustite in water–hydrogen gas mixtures. *J. Phys. Chem.* **69,** 327–334.

UREY H. C. (1952) *The Planets.* Yale University Press, New Haven, Connecticut, USA. 245 pp.